Temporal Characteristics of the Human Finger

by Ujjwal Singh

Research Project

Submitted to the Department of Electrical Engineering and Computer Sciences, University of California at Berkeley, in partial satisfaction of the requirements for the degree of **Master of Science, Plan II**.

Approval for the Report and Comprehensive Examination:

Committee:

Ron Fearing
Research Advisor

Date

* * * * * *

Frank Tendick
Second Reader

Date

Contents

Abstract

A stimulator display for the human tactile system needs to make use of both the spatial and temporal characteristics of the sense of touch. The temporal response of the human tactile system includes hysteresis or memory. We ran psychophysical experiments on human subjects to determine whether the finger exhibits a significant amount of hysteresis and how this affects the overall tactile system. Since most tactile stimulators include an elastic layer as an anti-aliasing filter, our tests were carried out with a layer of elastic material on the finger. There was a significant amount of memory in the finger which affected the perception of the inputs presented to the subjects. We offer a possible explanation for the results based on the mechanics of the skin.

1 Introduction

Tactile shape information is important for both object recognition and control purposes [Kon95]. Experiments by Johansson and Westling (1984) have shown that precision manipulation skills are severely reduced without tactile perception [PH96a]. Tactile shape information can be conveyed to an operator through a tactile display system.

Most tactile display systems use small pins or piston arrays indented into the skin surface to generate approximations to actual contours or surface stresses. The idea is that it is possible to perceive a shape or contour on the finger when the density of the pins is four times the spatial density of the mechanoreceptors in the skin [Tan95]. Valbo and Johansson (1979) found the spatial density of SAI mechanoreceptors in the skin to be 70 $sensors/cm^2$. This would require that the pins/pistons be spaced, at most, $1.2mm$ apart. A densely packed array of pins, with a $2.0mm$ spacing between piston centers, causes aliasing (individual pistons of the stimulator array are felt) [CLF92]. So, to create the sensation of a continuous surface, the pins/pistons must be brought closer together (limited by actuator size) or they can be spatially low-pass filtered to eliminate the aliasing effects. Therefore, most tactile display systems have an intervening layer of material (usually rubber) which acts as an anti-aliasing filter [Tan95]. We have used a rubber layer of thickness (see discussion in [Tan95]) $2.0mm$ for our filter. This thickness is chosen as a compromise between loss of sensitivity and anti-aliasing. The ideal display system also must have a temporal bandwidth comparable to the bandwidth of the mechanoreceptors in the human finger.

Neurophysiological studies by LaMotte and Srinivasan (1987) suggest that SAI mechanoreceptors are most important in small-scale shape perception. The SAI's have a field diameter of $3-4mm$, a frequency range of $DC-30Hz$ and sense local skin curvature [Kon95]. This suggests

that a relatively low bandwidth display might work for most applications. The SMA actuated display designed by Kontarinis has a bandwidth with a $-3dB$ point between $6-7Hz$ [Kon95]. Cohn et al. get a $7Hz$ frequency response out of their pneumatically actuated display. Both of these displays are well below the $30Hz$ bandwidth of the SAI mechanoreceptor. Since there are some physical limitations (such as hysteresis in SMA), display bandwidths might not increase in the near future (recently $50Hz$ bandwdith was achieved using SMA with ice water cooling [How97]). But performance improvements can still be made by exploiting the perceptual properties of the human finger.

In the visual world, terms such as refresh rates and frames/sec define the bandwidth of a visual display system. TVs and monitors are built to use the well known limitations of our visual system (*e.g.* interlaced scanning, minimum refresh rate of $70Hz$ for flicker free displays). This same principal can be applied to tactile display. If we had more information about the human tactile system, we could use it to build better displays (*e.g.* use interlaced scanning of the pins across the finger by using the memory in the finger). This paper tries to determine the limitations in dynamic human tactile perception that could be used to improve tactile display resolution.

1.1 Previous work

Many researchers have examined the mechanical properties of skin. Pawluk and Howe have used Fung's quasi-linear viscoelastic model of tissue to propose a viscoelastic model which describes the response of the human finger pad to mechanical deformation [PH96c], [PH96b]. They also showed that the finger pad can be described by a non-linear relationship between force and stiffness. Much of this work has also been done by Fung for soft tissues [Fun93]. Serina, Mote and Rempel have done studies on finger pad displacement for ergonomic purposes. They have shown that the bone, nail interface can be considered incompressible compared to the finger pad [PH96b].

There has been very little work done with temporal response of the human tactile perception. We could not find any work that dealt with *viscoelastic memory* in the human finger and how this affects the tactile perception. There has been some work done by VanDoren with spatiotemporal sensitivity [Dor89]. This model treats the finger pad as a linear Voigt body. The model he presents is valid for very low forces ($0.1N$). Verrillo and Chamberlain, as discussed by VanDoren, have done some temporal studies with the tactile system. But their work focuses on inputs with frequencies of $250Hz$ and higher [Dor90]. Tan's research to determine spatial sensitivity of the

human finger was affected by temporal properties of the finger. In his experiments, subjects reported that, after wearing the rubber gloves (anti-aliasing elastic layer) for some time, patterns became harder to discern. Some subjects claimed that they perceived grating patterns on two comparison surfaces, when in fact one was known to be smooth. Although he did not draw any quantitative conclusions, he hypothesized that the viscoelastic memory of the finger might be confusing the SAI mechanoreceptors. He states that the amplitude resolution capabilities of the human finger might be decreased by hysteresis causing errors in perception [Tan95].

1.2 Goals

This project attempts to determine if the viscoelasticity of the finger has some effect on the human tactile perception. We use a similar setup as Tan [Tan95] and conduct psychophysical experiments to determine if the viscoelastic memory can be quantitatively observed in human subjects. We also present a hypothesis to explain how this memory affects overall tactile perception.

2 Model of the human finger

In this section, we describe a static model of skin mechanics. This is the same static linear model used by Phillips and Johnson [PJ81] for finger skin and Fearing [Fea90] for robotic tactile sensors. It provides a simple model of the stresses and strains present at the finger as the inputs are applied. We also describe a linear viscoelastic model of the human finger pad based on work done by Fung. Fung's work can be used to accurately model the actual tissue beneath the skin. This model can be used to understand the effects of forces on the finger over time. The viscoelastic model is also a good model of memory or hysteresis (*viscoelastic memory)* present in the finger.

2.1 Model of skin mechanics

Using the work of Phillips and Johnson [PJ81], I develop a model for the finger that can be used to predict the strain at various depths in the skin under certain assumptions. While this model is grossly simplified and inaccurate under certain conditions, it is qualitatively useful and provides a good starting point for the analysis.

There are two assumptions that can be applied to planar elasticity problems. The *plane strain assumption* states that for an infinite line load on an elastic half space, the strain in the direction of

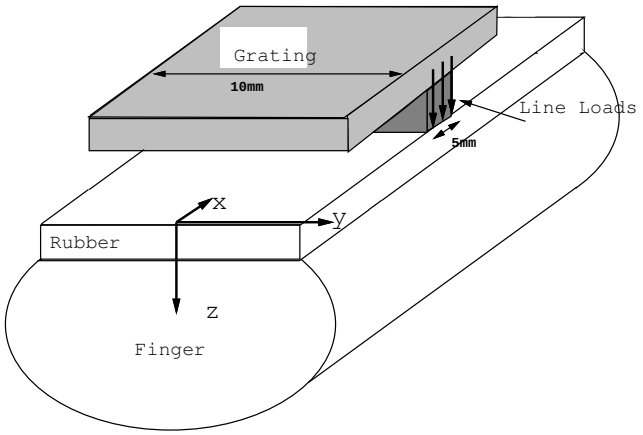

Figure 1: Finger and pattern geometry for plane stress assumption

the load must be zero. The *plane stress* assumption says that the stresses normal to a slice out of the elastic half plane must be zero [FH85]. Phillips and Johnson determined that the plane stress assumption leads to qualitatively better agreement between the response of the mechanoreceptors and the stress/strain relationship of the finger. So, I will use the plane stress model here.

Figure 1 defines the coordinate system and finger and pattern geometry for the plane stress assumption. The stresses due to contact with a raised ridge are modeled as normal line loads. They are constant in the y-axis (between 0 and $10mm$ in y-contact length) and have a square root (for cylindrical indentors) or inverse square root distribution (for rectangular indentors) along the x-axis of the finger (between $-2.5mm$ and $2.5mm$). A thin slice is taken from the x-z plane and is used for the following planar stress analysis. The plane stress assumption states that the stress σ_{y} is equal to 0 for a line load P. Following the analysis in [Tan95], and [PJ81], the normal component of the strain is:

$$\epsilon_{\mathrm{z}} = \frac{-2Pz}{E\pi r^4}(z^2 - \nu x^2) \tag{1}$$

In equation (1) above, P is the force per unit length (given in N/m), $r^2 = x^2 + z^2$, and ν is Poisson's ratio (0.5 for incompressible materials such as rubber), and E is defined as Young's modulus (which for our elastic rubber layer is $4 \times 10^5 N/m^2$). In our case the pattern is pressed

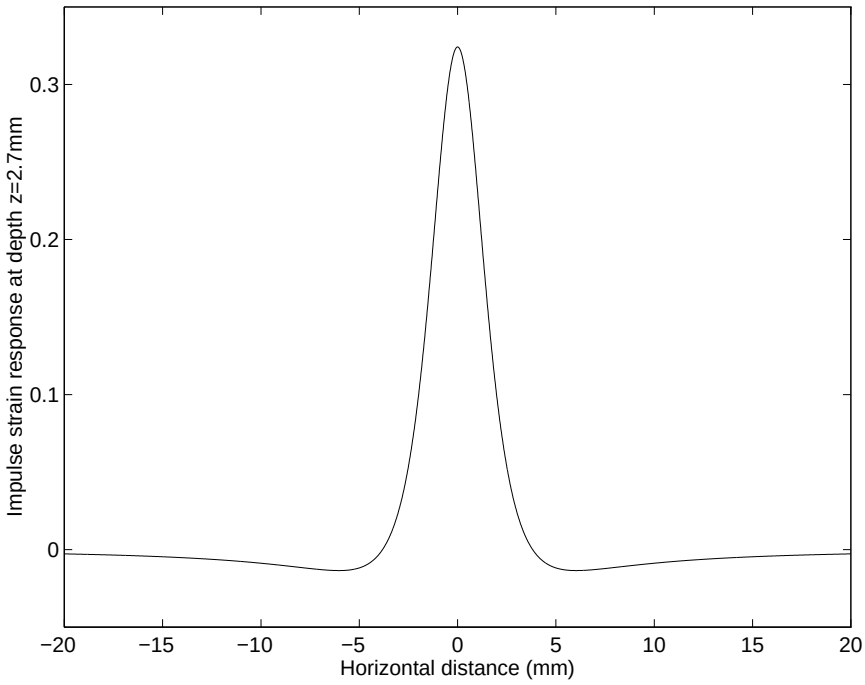

Figure 2: Impulse strain response at a depth of $z = 2.7mm$

against the finger with a force of $5.5N$ over a contact length of $10mm$, which means our $P = 550N/m$. Thus, the impulse strain response at a depth of d_0 can be calculated from the above equation 1 (note: we are assuming here that the E for the skin is the same as that of the rubber layer and d_0 includes the thickness of the rubber layer as well as the depth of the mechanoreceptors) and results in the following.

$$\epsilon_z(d_0, x) = \frac{-2Pd_0}{E\pi r^4}(d_0^2 - \frac{1}{2}x^2) \tag{2}$$

d_0 is taken to be $2.7mm$ (which corresponds to the $2.0mm$ rubber layer thickness and $0.7mm$ depth of the SAI mechanoreceptors in the skin). We assumed $0.7mm$ as the depth for the SAI mechanoreceptors because, as explained by Tan [Tan95], they were found at a depth of approximately $0.7mm$ to $1.0mm$ in macaque monkeys. The actual depth in humans is unknown and is probably quite variable between different people. But $0.7mm$ provides a starting point. Figure 2 shows the spatial impulse response of normal strain for a linear elastic medium in response to a line load.

We also need to determine what our pattern feels like on the finger. In other words, we need to determine the surface stresses for the pattern that is indenting the finger. Our patterns are

rectangular indentors that have been slightly rounded by sanding. While the exact stress profile is not known for this pattern, we do know that the stress profile will be "smoother" than the stress for a rectangular indentor yet "sharper" than the stress for the cylindrical indentor. This lets us bound the predicted maximum and minimum sub-surface strain.

Conway gives the surface stress for a rectangular indentor on an elastic half-plane as [Con66]

$$\sigma_z = \begin{cases} \frac{P}{\pi\sqrt{a^2-x^2}} & \text{for } |x| < a, \\ 0 & \text{otherwise} \end{cases} \tag{3}$$

where P is once again the force per unit length (equals $550N/m$ in our case) and a is the half width of the contact. Since the contact width corresponds to the width of the ridge on the pattern, $a = 2.5mm$ (See figure 1). The surface stress for a rectangular contact is shown on the top left in figure 3. Note, there is a discontinuity in the stress at the tip of the rectangular contact, where the edge of the ridge meets the finger.

The surface stress for a rigid cylinder indenting an elastic half-plane is also given by Conway [Con66] as:

$$\sigma_z = \frac{2P}{\pi a^2}\sqrt{a^2 - x^2} \tag{4}$$

and it is shown on the top right in figure 3. In this case, a is the half-width of the contact region and is a function of the radius of the cylinder. We have assumed $a = 2.5mm$. We don't expect to see any infinite stresses (as we do in the top left figure 3 for rectangular indentations). Instead, we see that the peak value of the stress is at the center of the contact and approaches zero at the edges.

Now the strain at a depth of $2.7mm$ below the skin (we also have included the $2.0mm$ thickness of the rubber layer) is simply the convolution of the above stresses with the strain impulse response shown in figure 2. The strain at a depth of $z = 2.7mm$ is shown in figure 3. The cylindrical contact results in a higher strain (a little over 12%) at the center of the contact area. The strain profile for our single ridge will actually lie "in between" the strain profiles of figure 3, since the edges were slightly rounded.

There are several things to note about the above model. In the model, it is assumed that the anti-aliasing filter and the skin form one continuous layer with a modulus of elasticity of $4 \times 10^5 N/m^2$. However, this is not a valid assumption. Since the skin's modulus of elasticity is much lower than the rubber's, there is a boundary between the two surfaces (the elastic layer and the skin). One could get around this problem by using finite element analysis (FEA). FEA would work quite well since,

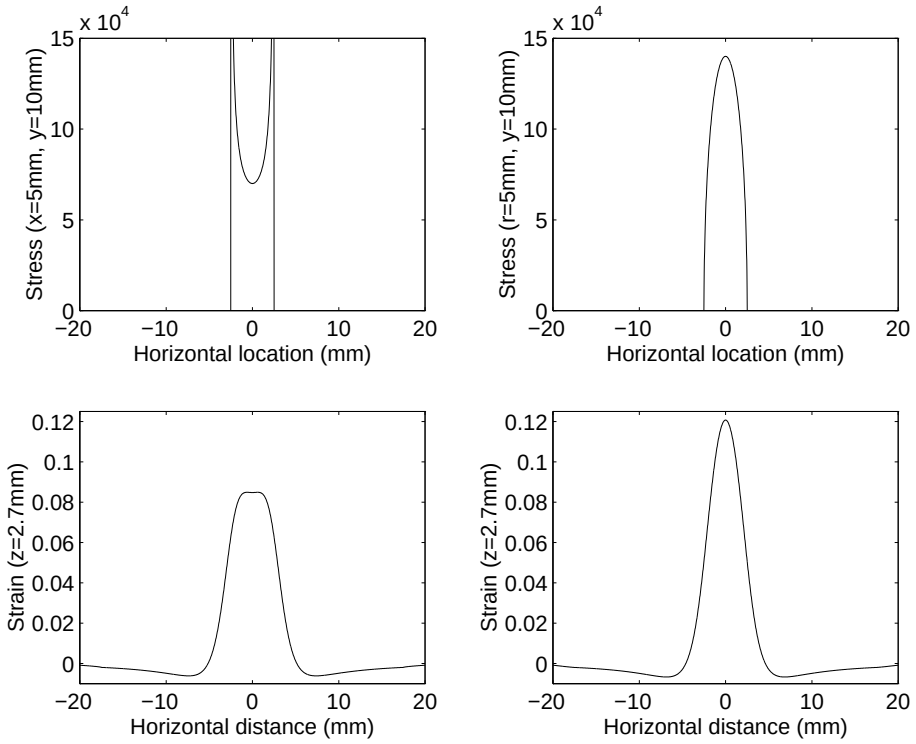

Figure 3: Surface stress and sub-surface ($z = 2.7mm$) strain profiles for rectangular and cylindrical indentors

as we will discuss below, there are good models for the actual tissue beneath the skin [Fun93], [PH96c]. However, it is much easier to see the effects of parameter changes using the analytic half-plane models. Furthermore, the work of Serina, Mote, and Rempel [SJR95] has shown that the bone structure acts like an incompressible barrier. Although our model did not use the above information, the half-plane elastic model is a good first order assumption and it does correspond to physiological measurements made by Phillips and Johnson [PJ81].

2.2 Viscoelastic model of skin tissue

Fung concludes [Fun93] that biological tissues are not elastic. The history of strain affects the stress (*viscoelastic memory*). There is a considerable difference in stress response to loading and unloading. This has lead to work in characterizing soft tissues using linear viscoelastic models. It is reasonable to assume that for oscillations of small amplitude about an equilibrium state, the theory of linear viscoelasticity should apply. Most of the research has concentrated on relating stress and strain in the soft tissue using Voigt, Maxwell, and Kelvin models [Fun93].

A *viscoelastic* material exhibits features of hysteresis, relaxation, and creep. *Hysteresis* is defined as the difference in the stress-strain relationship during loading and unloading. *Creep* refers to the fact that when a body is subject to a force step, and the force is maintained, then the body continues to deform. Finally, *stress relaxation* refers to the property that when a position step is suddenly applied to a body and then that deformation is maintained constant afterward, the corresponding stresses in the body decrease with time. We will concentrate on stress-relaxation in this study.

Viscoelastic materials are often discussed in terms of mechanical models. The three most commonly used mechanical models are the *Maxwell model,* the *Voigt model,* and the *Kelvin model,* all of which are composed of mechanical components such as springs and dashpots. A spring produces instantaneous deformation proportional to the load and a dashpot produces velocity proportional to the load. The Kelvin model (also known as the standard linear model) is the most general relationship that includes the load, the deflection, and their first derivatives. We decided to use the Kelvin model to explain the viscoelastic behavior of the human finger pulp.

The Kelvin model is shown in the figure 4. It consists of a series connection of a dashpot (with viscosity R) and a spring (with spring constant k_1) in parallel with another spring (with spring constant k_0). The Kelvin model is basically the Maxwell model in parallel with a spring.

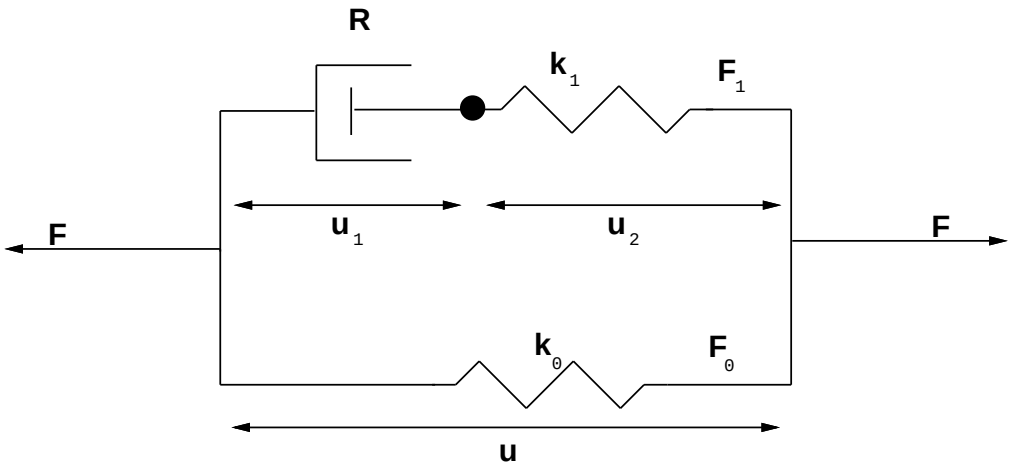

Figure 4: A Kelvin body (a standard linear solid).

In figure 4, the u refers to the displacement (u_1 for the dashpot and u_2 for the spring in series and the F is the total force (sum of the force F_0 from the spring and F_1 is the force from the Maxwell element). The differential equation relating the force and the displacement is given by [Fun93]

$$F + \tau_\epsilon \dot{F} = E_{\mathrm{R}}(u + \tau_\sigma \dot{u}) \tag{5}$$

with initial condition

$$\tau_\epsilon F(0) = E_{\mathrm{R}} \tau_\sigma u(0) \tag{6}$$

where τ_ϵ (called the *relaxation time for constant strain*), τ_σ (*relaxation time for constant stress*), and E_{R} (*relaxed elastic modulus*) are all functions of R, k_0, k_1. Solving equation 5 with the initial condition (equation 6 and $u(t) = 1(t)$ (unit-step function), we obtain the relaxation function (as $F(t) = k(t)$) [Fun93]

$$k(t) = [E_{\mathrm{R}} - \frac{E_{\mathrm{R}}(\tau_\epsilon - \tau_\sigma)}{\tau_\epsilon} e^{\frac{-t}{\tau_\epsilon}}]1(t) \tag{7}$$

The form of the relaxation function is shown in figure 5. Solving equation 5 with the same initial conditions and $F(t) = 1(t)$, we get the elongation produced by a sudden application of a constant force. This is called a creep function and is shown in figure 6 and is represented by equation 8.

$$c(t) = [\frac{1}{E_{\mathrm{R}}} - \frac{(\tau_\sigma - \tau_\epsilon)}{E_{\mathrm{R}} \tau_\sigma} e^{\frac{-t}{\tau_\sigma}}]1(t) \tag{8}$$

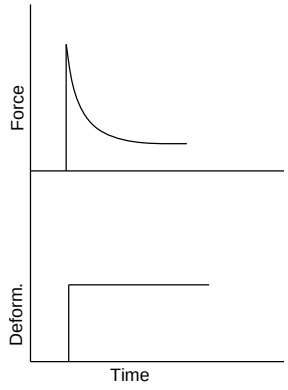

Figure 5: Relaxation function for a Kelvin body.

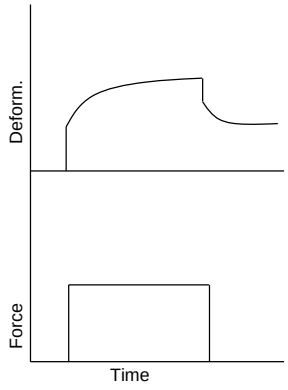

Figure 6: Creep function for a Kelvin body.

According to both Fung [Fun93] and Pawluk [PH96c], the nonlinear stress-strain characteristics of the living tissues must be accounted for. There have been several efforts in this direction most notably by Viidik (1966) who proposed a model based on the above Kelvin model and by Fung who proposed a quasi-linear viscoelastic model. Viidik's model is based on a sequence of springs in a Kelvin model of different natural lengths, with the number of springs increasing with increasing strain. Fung's quasi-linear viscoelastic model consists of two components: an elastic response, which is the instantaneous response of the finger to a position step; and, the reduced relaxation function, which is the normalized, time varying response of the finger to a position step [Fun93]. Pawluk and Howe have used this model and fitted it successfully to experimental results. Their results show that Fung's quasi-linear viscoelastic model is very successful in predicting the force output of the finger for new mechanical stimuli [PH96c]. But for our project, it was sufficient to use the simpler Kelvin model to see the viscoelastic memory effect.

3 Experimental Methods

We developed a system where patterns could be presented to test subjects in a controlled manner. The system had to provide accurate force and position control. Our experiments required fine control over the timing of when different patterns were presented as well as when force and position values were read. In this section, I will describe the apparatus and the experimental procedure used.

3.1 Apparatus

As mentioned above, we developed a system that allowed us to easily and quickly interchange test patterns and control and measure forces and positions. The robot modules of the Robotworld system in the EECS Robotics Lab at the University of California, Berkeley, were used as the top level controlling mechanism. There are four robot modules on the Robotworld system and each module has 4 degrees of freedom (x, y, z, and, θ). The robots were controlled in real time using device drivers running on a 68040 processor running LynxOS 2.0 [Nic94]. It was possible to move the modules in both position and force control mode. We used a Lord 15/50 Force/Torque sensor directly attached to the module. Again, there were real time device drivers for reading from the force/torque sensor. There were also two momentary switches (as well as accompanying real-time device drivers) placed within easy reach of the apparatus to record the responses of the subjects.

The entire apparatus was hidden from the view of the test subject. For each of the procedures outlined in section 3.2, the subject had his or her right index finger on a ledge with the palm of the hand facing towards the module. The module moved a plate containing wax blocks towards the finger. There was a $2.0mm$ rubber fingertip around the index finger. The robot module moved the plate until a block came in contact with a subject's finger pulp. The plate, blocks, and the rubber fingertip are described in the sections below. Figure 7 shows the complete apparatus used during the experiment.

3.1.1 Plate and blocks

The patterns presented to the subject consisted of blocks, each of which had a ridge or was smooth. The blocks were made with machinable wax blocks with a ridge milled onto its surface. The surface of the wax blocks were first smoothed down. Then a ridge, whose height varied from block to block, was milled onto the surface using small end mill cutters. The heights of the ridge varied from $0.1mm$ to $1.5mm$. Each ridge on the different blocks had a width of $5mm$ (figure 7) and the blocks came in contact with the finger in such a way that the length of the contact along the ridge was approximately $10mm$ (figure 1). There were also blocks that had no ridges (again the contact length on the finger was $10mm$). A rectangular plate was constructed and attached to the force/torque sensor for easy manipulation of the wax blocks. The plate had three stair-step grooves (see figure 7) cut into it where the wax blocks could be placed. Note, we used a stair-step configuration on the plate to ensure that the blocks had normal contact with a subject's finger and at the same time only the block being presented came in contact with the finger pulp. During a test, the index finger of the subject was placed on a ledge with the pulp facing out (so that the nail rested against the back of the ledge). The robot module was rotated to guarantee that the wax blocks would make normal contact with the finger. Each subject wore a rubber glove on his or her index finger.

3.1.2 Rubber glove

A $2.0mm$ thick rubber glove was fitted on the index finger of each subject. The gloves were manufactured with silicone rubber using the process described in [Tan95]. They were used in the experiments for several important reasons.

As mentioned in section 1, it is necessary to spatially low-pass the information from the

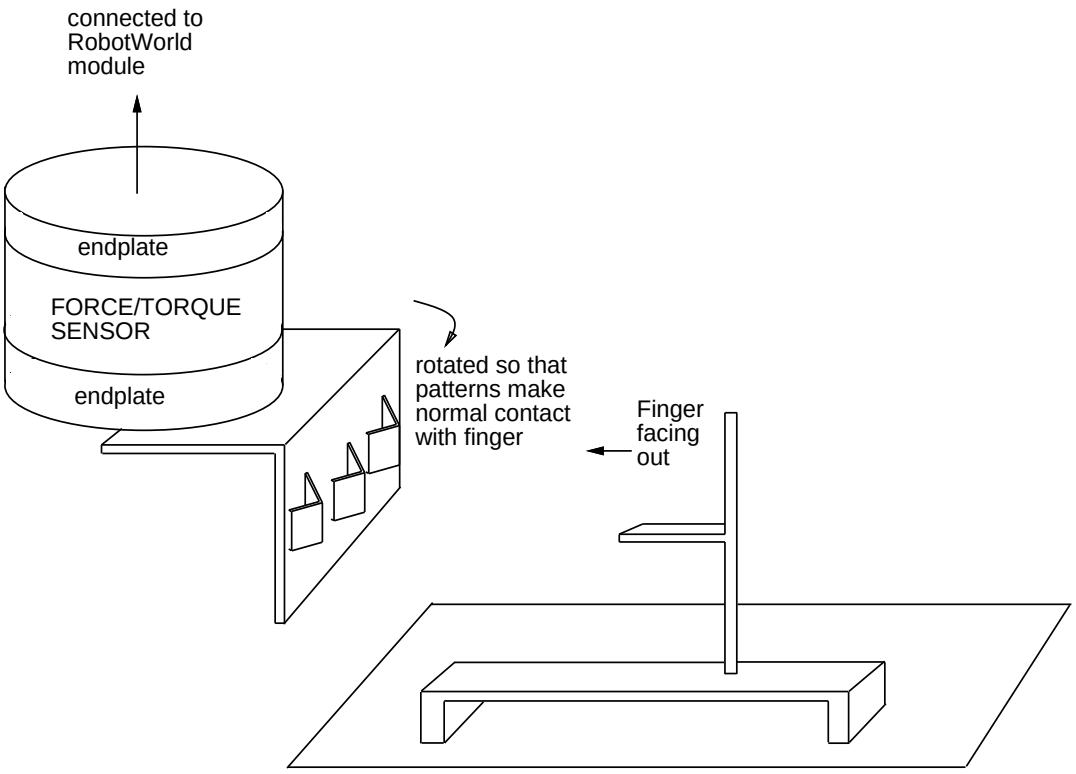

FRONT VIEW

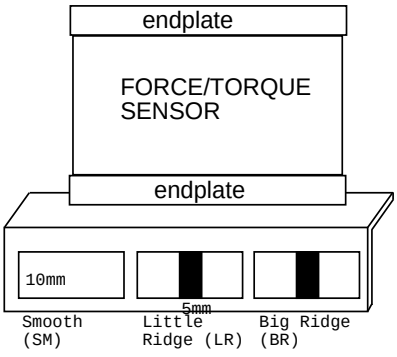

Figure 7: Testing apparatus

pins/pistons of a tactile display to create the sensation of a continuous surface. The rubber glove acts as a good anti-aliasing spatial low-pass filter. The rubber glove has to be thick (Fearing and Hollerbach [FH85] suggested that the rubber thickness should be twice the tactile array spacing) to remove the aliasing but it must be thin so that the finger retains good sensitivity. The $2.0mm$ thickness is chosen as a compromise between loss of sensitivity and getting a good anti-aliasing filter. The wax blocks that were presented as inputs to a subject's finger had varying textures and different thermal signatures. One could obtain additional information from these surface texture and temperature cues. The rubber glove as a low-pass filter removed these surface cues.

As described in section 3.2.2, the little ridge input (ridge height was either $0.1mm$ or $0.15mm$) was used after a big ridge input had been applied to the finger. We wanted the little ridge input to be ambiguous (i.e. at a 50% threshold level) to perceive for our experiments. Without the rubber glove, the ridge heights would have to be much lower than $0.1mm$ for the little ridge inputs to be perceived as ambiguous.

3.2 Procedure

Our goal was to determine if there was evidence for an effect of finger viscoelasticity on tactile perception. Therefore, we had to design experiments which measured both the viscoelastic effect as well as its effect on touch. Section 3.2.1 discusses the experiment used to verify the linear viscoelastic model of the finger and obtain its parameters. Section 3.2.2 describes the experiment used to obtain quantitative evidence of the effect of viscoelasticity on tactile perception.

3.2.1 Determining Viscoelasticity

We determined if the finger responded as described by equation 7. As described in section 2.2, we applied a position step to the finger and measured the finger's force response to compare it with the relaxation function shown in figure 5. The robot module was commanded to a position that corresponded to a force of $2.5N$ (measured by the force/torque sensor) exerted on the finger by the block containing the biggest ridge (this corresponded to blocks with ridge heights of $0.7mm$ or $1.0mm$). After fifteen seconds, during which the force response of the finger was recorded by the sensor, a position step of $0.05cm$ towards the finger was applied by the robot. The force/torque sensor recorded the force for thirty seconds. Finally, the module was commanded to move back to its original position (i.e. a negative step of $0.05cm$) and the sensor recorded the force for

another fifteen seconds. Due to the limited velocity of the robot module, the position step was not instantaneous. It took on the order of $0.6 - 0.7 seconds$ to move the $0.05cm$. The above procedure gave us a relaxation curve for each subject which was used to estimate the parameters of the Kelvin model (parameters of equation 7). The results and analysis are discussed in section 4.

3.2.2 Effect on Tactile Perception

In the second part of the experiment, we determined if the viscoelasticity of the finger pulp had a statistically significant effect on the perception of ridges on the wax blocks. The plate was set up with three blocks. The leftmost block (in figure 7) was smooth (SM) block (had no ridge). The middle groove contained a block with a little ridge (LR) whose height was either $0.1mm$ or $0.15mm$. The height of the LR for each subject was determined before the experiment started. It corresponded to the ridge height that was just at threshold through the $2.0mm$ glove. The threshold point was defined to be the ridge height at which the subjects were guessing whether they had felt a ridged pattern (i.e. there was equal chance of a subject guessing that he/she had felt a smooth pattern). The third groove on the plate in figure 7 had the block containing a big ridge (BR). The BR block was the same as the block used in the viscoelastic test (3.2.1) to measure the relaxation function of a subject. The robot module was commanded to move the plate to the finger until the block being presented as stimulus applied a force of $5.5N$ on the finger (as measured by the force/torque sensor). The ordering and the timing of stimulus was controlled very carefully and is described below.

The experiment consisted of 150 trials broken up into five sessions (thirty trials per session). Each trial consisted of two blocks being presented to the subject. Each trial was one of five types outlined in the table 1. Note, with three different blocks, each trial could have been one of nine (3^2) different types (since two blocks were being presented in each trial). But we only used the combination of blocks that were important (to cut down on the number of trials) in showing whether or not the viscoelasticity of the finger had an effect on touch. The set of 150 trials was generated randomly prior to the experiment. They were generated in such a way that there was a set of thirty trials of each type in the experiment. Thirty trials were picked because the normal approximation (using the central limit theorem) is a good approximation regardless of the shape of the population if the sample size is greater than or equal to thirty [WM93]. Furthermore, since the experiment was carried out over five sessions (a session consisted of thirty trials), each session had six trials of

Type	First Stimulus	Second Stimulus
1	SM	BR
2	SM	SM
3	BR	SM
4	LR	BR
5	BR	LR

Table 1: Trial types and corresponding patterns presented (SM=Smooth, LR=Little Ridge, BR=Big Ridge).

Choice/Button	Condition(s)
1	Neither input had ridges,
	Only one input had ridge,
	Input(s) had negative ridges (grooves)
2	Both inputs in the trial had positive ridges

Table 2: Choices and condition(s) for each choice

each type.

In each trial, the robot module presented the first stimulus with a force of $5.5N$ for exactly 3 seconds at which point the module moved away from the finger and waited for exactly 1.8 seconds (1.8 was picked because it was determined from the first experiment that the average relaxation time constant for the subjects was approximately 2 seconds). Following the wait, the second stimulus was presented (also at $5.5N$) for exactly 2 seconds. The subjects were asked to push the appropriate button (momentary switch) based on whether or not they felt two ridges in the trial (i.e., felt ridges on both the stimuli). The conditions for when the subjects were supposed to push each button is outlined in table 2. The subjects had 10 seconds within which to make a choice. In other words, the time between each trial was held constant at 10 seconds. The results were compiled and are analyzed in section 4.

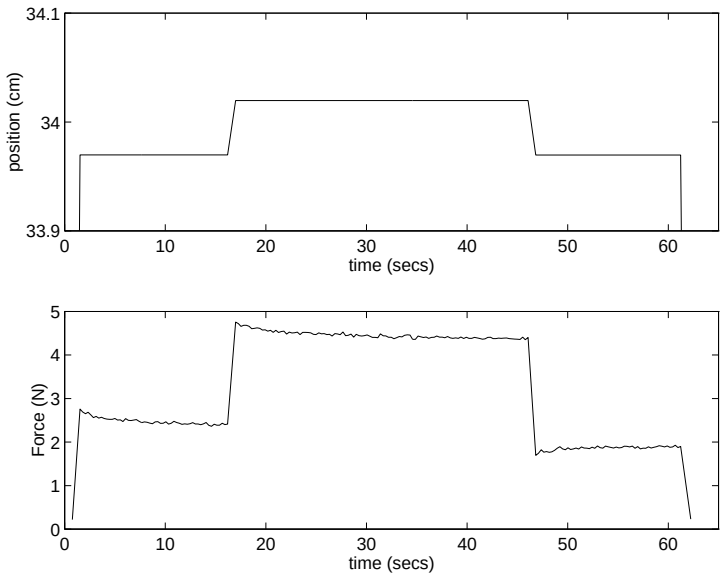

Figure 8: Relaxation function for a rubber layer.

4 Results

The experiments were run on six test subjects, 3 male and 3 female. All subjects were volunteers and no special criteria were used to select them. Two subjects were familiar with the experimental apparatus and procedure, while the other four subjects had no prior knowledge. The ages of the subjects varied from 21 to 35 years of age. The following is the performance and analysis of each of the six subjects.

4.1 Viscoelasticity

We showed in section 2.2 the finger mechanical model consisting of springs and dashpots. After running the first experiment, a relaxation function was obtained for each of the six subjects. Figure 8 shows a relaxation function (to a position step) for a rubber layer. Note, one can see a very small viscoelastic effect here. Figure 9 shows a relaxation function for one of the subjects (subject 2). The viscoelastic effect is very apparent up to approximately 15 seconds (just before the $0.05cm$ position step). The other subjects exhibited similar relaxation functions. The relaxation function for the Kelvin, equation 7, can be rewritten more generally as

$$k(t) = A + Be^{-tc} \text{ where } A = E_{\mathrm{R}},\ B = \frac{-E_{\mathrm{R}}(\tau_\epsilon - \tau_\sigma)}{\tau_\epsilon},\ \text{and } c = \frac{1}{\tau_\epsilon} \tag{9}$$

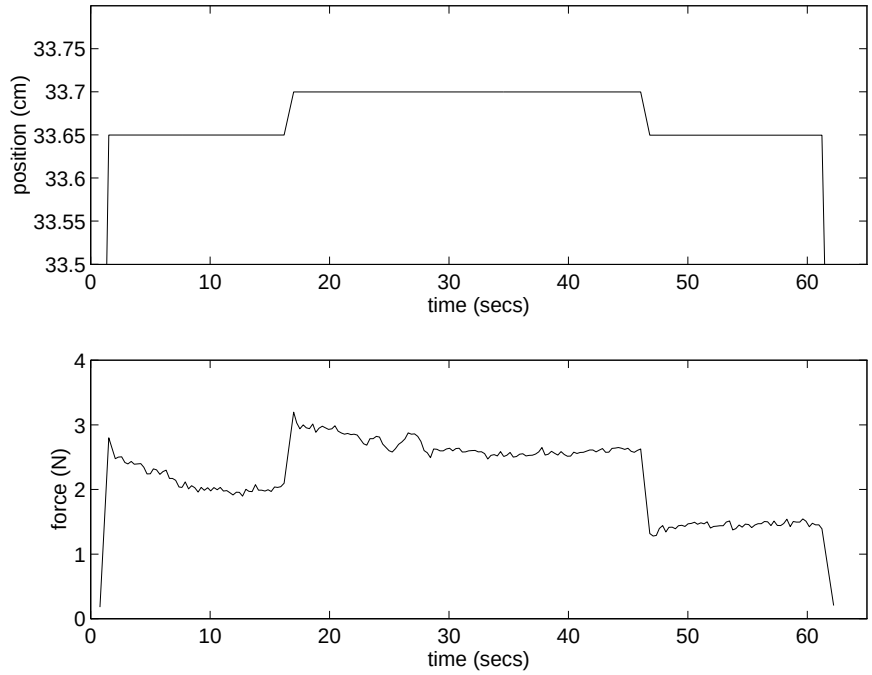

Figure 9: Relaxation function for one of the subjects (subject 2).

We used MATLAB (using a nonlinear curve fitting algorithm based on the simplex algorithm) to fit an exponential function of the form given in equation 9 to the force response taken in the first 15 seconds for each subject. Figure 10 shows an example of the curve fitting for the relaxation curve of the subject shown in figure 9 which corresponds to subject 2. The data for the other subjects is shown in table 3. Note, the value τ_σ can be found by substituting the known values into the equation for B in equation 9.

According to equation 8, and figure 6, after the constant force input is removed, the finger pulp (because of the viscoelastic creep) exponentially deforms back to its original location, with time-constant equal to τ_σ (we will ignore all other constants for this analysis). When a BR pattern is pressed against the finger with a force of $5.5N$ for 3 seconds, then the deformation is equal to one (arbitrarily normalized units-zero corresponds to the finger pulp in its original location). 1.8 seconds after the pattern is removed, the finger will be at some position depending on the value of τ_σ for each subject. Table 4 shows the deformation (in the above normalized units where zero corresponds to the finger in its original location, and one corresponds to the location of the finger after a BR pattern has been pressed on it for 3 seconds) for each subject 1.8 seconds after the BR pattern is removed. A smaller number means that the finger is closer to its original location. In other words, subject 1's finger pulp is only 43% away from its starting location, whereas subject 2's

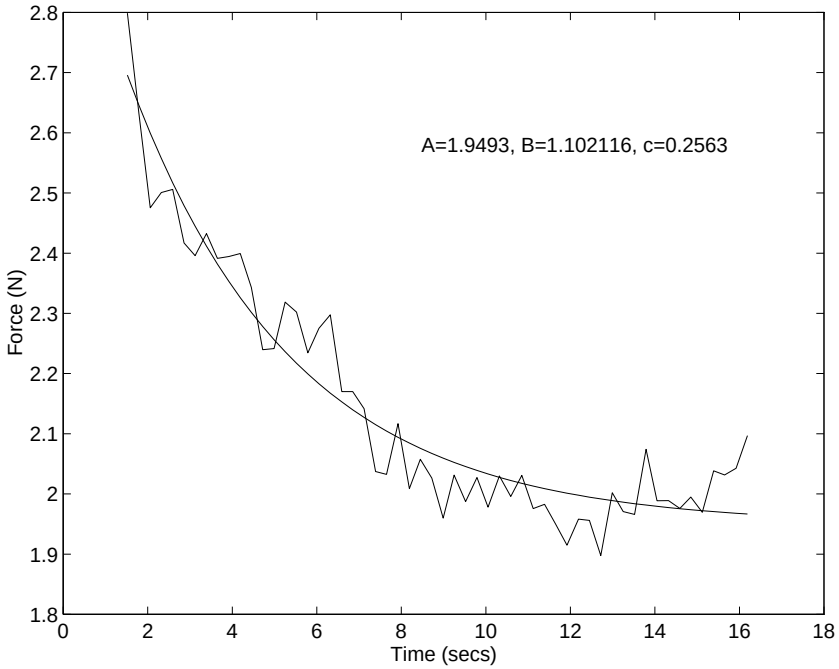

Figure 10: Exponential fit for relaxation function.

Subject	A	B	c	τ_ϵ	τ_σ
1	2.29	1.15	0.70	1.42	2.14
2	1.95	1.10	0.26	3.90	6.11
3	2.20	0.89	0.58	2.71	3.82
4	2.24	0.67	0.35	2.81	3.65
5	2.04	0.85	0.30	3.38	4.78
6	2.59	0.34	0.26	3.88	4.39

Table 3: Parameter values of the viscoelastic model of the finger

Subject	Position of finger
1	0.43
2	0.74
3	0.62
4	0.61
5	0.69
6	0.66

Table 4: Position of finger 1.8 seconds after a BR pattern is applied (in normalized units where zero corresponds to finger in starting location, and one corresponds to location of finger after a BR pattern has been pressed on it for 3 seconds

finger pulp is 74% from its original location. Equivalently, we can think of this as the finger pulp retaining some memory of the input even after 1.8 seconds. The first subject's finger remembers 43% of the input while the finger on the second subject remembers 74% of the input.

4.2 Effect on perception

The second experiment was run on all six subjects. As mentioned earlier, the responses of the second experiment were either $choice1$ (if a subject did not feel a ridge on each of the two inputs of the trial) or $choice2$ which corresponded to a subject feeling two ridges in the trial (see table 2). The performance, as indicated by fraction of trials that a subject picked $choice2$ for each type of trial, is shown in figure 11. Refer to table 1 to see what input patterns were presented for each type.

Looking at figure 12, we see that for trials of types 4 and 5, the fraction of trials for which subjects picked $choice2$, seems to be different. What we needed to determine is whether or not the difference in the the two fractions was statistically significant. In other words, what was the confidence level with which we could say that the means (fractions) of the response of $choice2$ were different for each of the trial types. To accomplish this, we used a modified pooled t-test (sometimes called the two sample t-test). The pooled t-test is often used when comparing two means whose variances are unknown but equal. In our case, we wanted to compare the mean response of $choice2$ for trials of type 4 (p_1) and type 5 (p_2) for each subject. The variance of

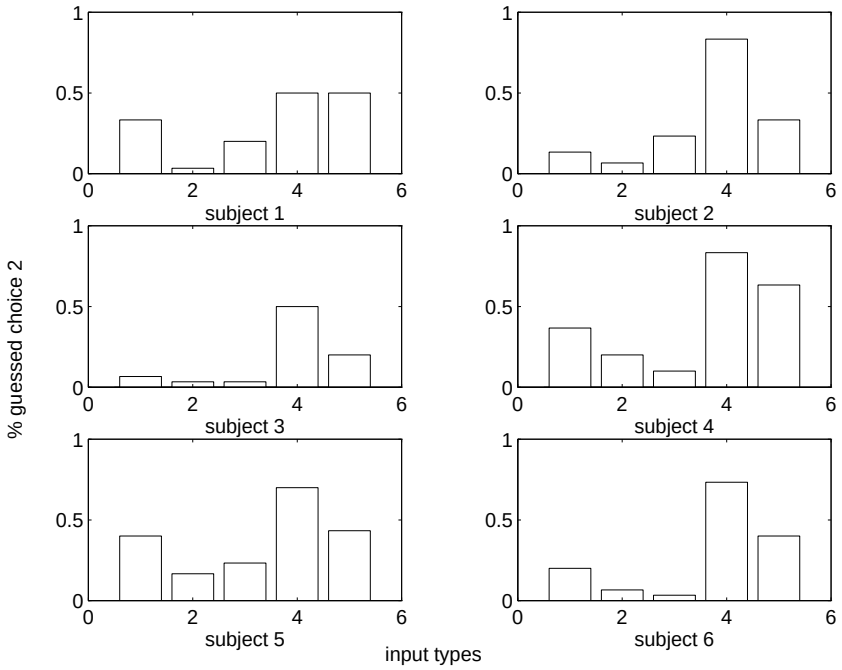

Figure 11: Fraction of trials of all types (1=(SM,BR), 2=(SM,SM), 3=(BR,SM), 4=(LR,BR), 5=(BR,LR)) for which 'felt two ridges' (choice 2) was picked as a response.

$choice2$ responses for type 4 was not equal to the variance of the responses for type 5. Thus, we had to use a modified pooled t-test which is described in section 4.2.1.

4.2.1 Statistical Comparison of Means

We want to show that p_1, which is equal to the mean for type 4 inputs (in other words, it is the fraction of trials of type 4 for which the response was $choice2$), is not equal to mean for type 5 inputs (p_2). We also wanted to see if we could state this with 95% confidence interval for each of the subjects.

We begin by formulating the null hypothesis (H_0) and the alternative hypothesis (H_1). We know that a firm conclusion can only be made if a hypothesis is rejected. We would like to say that $p_1 \neq p_2$, or in other words, we would like to reject the hypothesis that $p_1 = p_2$. Therefore, in our case we form the null hypothesis and alternative hypothesis as outlined in equation 10.

$$\begin{aligned} H_0 : &\quad p_1 - p_2 = 0 \\ H_1 : &\quad p_1 - p_2 \neq 0 \end{aligned} \tag{10}$$

The two-sample t-test may be used when we can assume that both distributions are normal

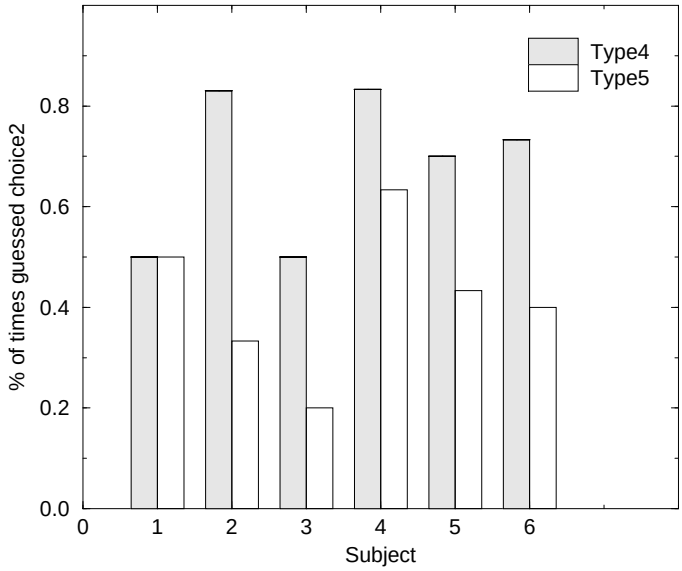

Figure 12: Fraction of trials of types 4 (LR,BR) and 5 (BR,LR) for which 'felt two ridges' (choice 2) was picked as a response

(which is a valid assumption in this case because the number of samples equals thirty which implies we can use the central limit theorem). In our case, we have two means, but we do not have the variances. Furthermore, we can safely assume that the variances of each of the distributions are not equal. Therefore, we use the modified two-sample t-test which uses sample variances. The sample variance can be calculated for the distribution of responses for type 4 and type 5 trials as outlined in equation (11).

$$\sigma^2 = \frac{\sum_{i=1}^{n}(x_{\mathrm{i}} - \bar{x})^2}{n-1} \tag{11}$$

The value of the test statistic is given by equation 12

$$\begin{aligned} t' &= \frac{\bar{x_1} - \bar{x_2}}{\sqrt{\frac{\sigma_1}{n_1} + \frac{\sigma_2}{n_2}}} \\ \nu &= \frac{(\frac{\sigma_1}{n_1} + \frac{\sigma_2}{n_2})^2}{\frac{(\sigma_1/n_1)^2}{{n_1}^{-1}} + \frac{(\sigma_2/n_2)^2}{{n_2}^{-1}}} \end{aligned} \tag{12}$$

The means, sample-variances, and t-values for each subject are shown in table 5.

The critical region for the test is defined by equation (13) where α is the probability of a type I error (i.e. rejection of the null hypothesis when it is true). It is also referred to as the level of

Subject	Type	Not two ridges	Two ridges	% Two ridges felt	Sample σ^2	t-value	ν
	4 (LR-BR)	15	15	0.50	0.26		
1	5 (BR-LR)	15	15	0.50	0.26	0	58
	4 (LR-BR)	5	25	0.83	0.14		
2	5 (BR-LR)	20	10	0.33	0.23	*4.48*	55.1
	4 (LR-BR)	15	15	0.50	0.26		
3	5 (BR-LR)	24	6	0.20	0.17	*2.52*	55.3
	4 (LR-BR)	5	25	0.83	0.14		
4	5 (BR-LR)	11	19	0.63	0.24	1.77	54.5
	4 (LR-BR)	9	21	0.70	0.22		
5	5 (BR-LR)	17	13	0.43	0.25	*2.13*	57.6
	4 (LR-BR)	8	22	0.73	0.20		
6	5 (BR-LR)	18	12	0.40	0.25	*2.72*	57.4

Table 5: Raw data and t-values for each subject

significance.

$$\begin{aligned} t' &< -t_{\alpha/2} \\ t' &> t_{\alpha/2} \end{aligned} \tag{13}$$

At a level of significance of 0.05 (i.e. 95% confidence level), we can determine the critical values of the t-distribution. For our values of ν and α equal to 0.05, it was determined that the critical value $t_{\alpha/2}$ was equal to approximately 2.000. At a significance level of 0.10, the critical value was equal to 1.671. From this we can safely conclude that the the means for trials of types 4 and 5 were not equal for subjects 2, 3, 5, and 6. Subject 4 fell within the 0.10 level of significance. Subject 1's means were equal. This data is explained in section 5.

5 Discussion

In section 5.1, I present a hypothesis to explain the effect of viscoelastic memory on tactile perception. In section 5.1.1, I show the relationship between Kelvin's linear viscoelastic model and the effect on tactile perception. Section 5.1.2 gives an approximate explanation of the effect

of viscoelastic hysteresis on perception in terms of the skin mechanics as discussed in section 2.1. Section 5.2 discusses some sources of error present in the experiment. Finally, section 5.3 deals with future work and extensions to the work presented here.

5.1 Conclusion

5.1.1 Skin Viscoelasticity and Perception

In section 4.1, we determined the parameter values of the linear viscoelastic model of the finger for all the subjects. Table 3 shows all the parameters of the Kelvin viscoelastic model for all six subjects. Table 4 shows the position of the finger pulp 1.8 seconds after a big-ridge pattern is applied to the finger pulp with constant stress. As mentioned earlier, this is also an indication of memory of the input retained by the finger pulp.

In our experiment to measure effect on perception (section 3.2.2), each of the inputs was applied to finger with a constant force (i.e. each input exerted a constant stress on the finger pulp). Therefore, the important viscoelastic parameter for our case is τ_σ—relaxation time for constant stress. Figure 13 shows the relationship between the effect on tactile perception and the percent deformation retained by the finger 1.8 seconds after BR input is applied with constant stress. The deformation retained by the finger is caused by the viscoelasticity of the skin and is directly related to τ_σ (as discussed in section 4.1). The effect on perception is "measured" as the difference between the choice2 (two positive ridges felt) means for type 4 trials (LR,BR) and choice2 means for type 5 trials (BR,LR). This can be thought of as a measure of memory or hysteresis in tactile perception. Figure 13 shows that there is a linear relationship between the percent deformation retained by the finger and hysteresis. Subject 1 retains the least amount of finger deformation (only 43%) and also shows no hysteresis with the experiment's time scale. Subject 2's finger still retains 74% of its maximum deformation, 1.8 seconds after being indented by a BR pattern, and exhibits the largest amount of memory in tactile perception.

5.1.2 Skin Mechanics and Perception

In section 2.1, we determined the surface stresses and sub-surface strains for a ridged pattern indenting the finger. Figure 3 shows the stresses and the sub-surface strains for rectangular and cylindrical indentors. As it was mentioned, the stresses and strains of figure 3 were just the

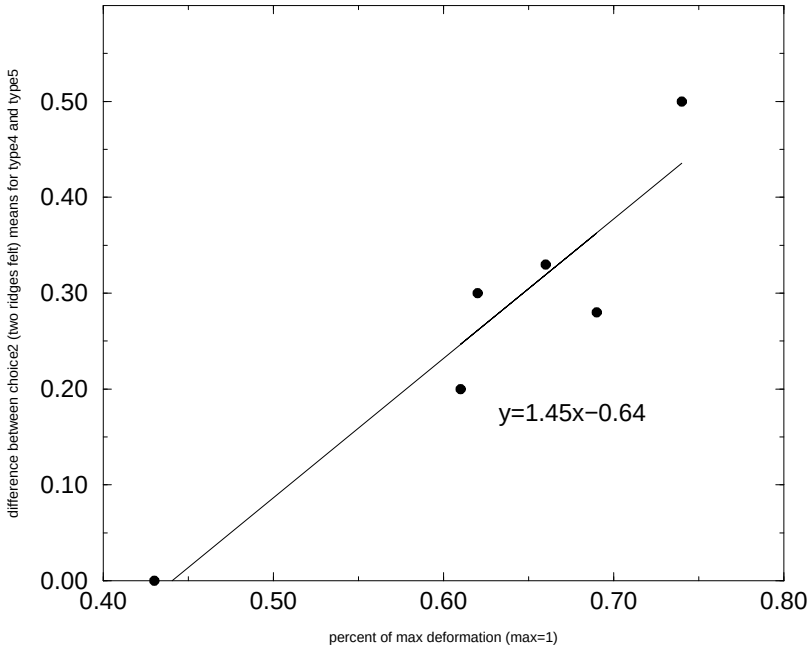

Figure 13: Difference of choice2 (two ridges felt) means for trials of type4 and type5 vs. percent of max deformation retained 1.8 seconds after BR input

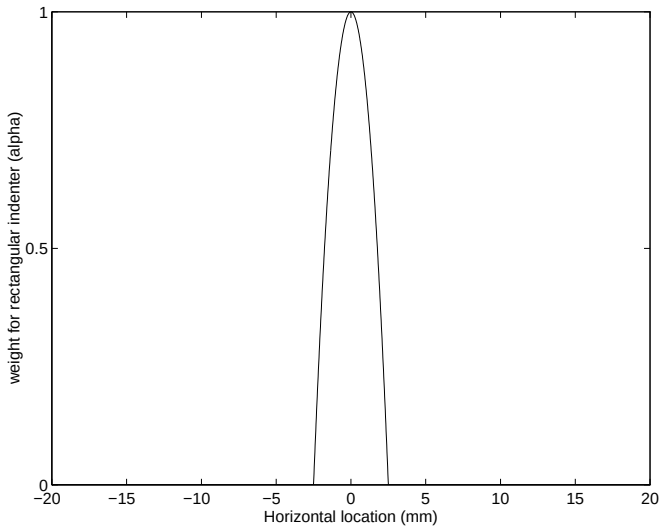

Figure 14: Weighting on the rectangular indenter

maximum and minimum bounds for the actual stress and strain felt for contact with the ridged pattern. Therefore, we first determine the stresses and strains for each of the input types (big-ridge (BR), little-ridge (LR), and smooth (SM)).

The BR pattern had its ridge slightly smoothed. The center of the ridge was primarily rectangular but it was rounded on the edges of the ridge. Thus, the BR pattern was modeled as a linear combination of rectangular and cylindrical indentors. We assume for small indentation that getting stress from shape is a linear, space-invariant operation. Therefore using superposition, the stress profile for our BR pattern was a weighted combination of the stress profiles for the rectangular and cylindrical indentors. The weighting was necessary for the following two reasons:

- The big-ridge was more rounded (cylindrical) at the edges than in the center.
- The total load under the big-ridge stress profile has to remain constant ($5.5N$).

We used a weighting function as shown in figure 14. The weighting function gives the multiplicative factor for the rectangular indentor. It is zero at $-2.5mm$ and $2.5mm$. These points correspond to the edge of the ridge. The weighting function has a maximum value at the center of the ridge. This satisfies the first point above (the edges of the ridge were modeled as cylindrical contact while the middle of the ridge was modeled as a rectangular contact). To ensure that the load under the BR stress profile integrates to $5.5N$ (second point above), we used the following formula:

$$\sigma_{\text{br}}(x) = w(x)\sigma_{\text{rect}}(x) + (1 - w(x))\sigma_{\text{cyl}}(x) \tag{14}$$

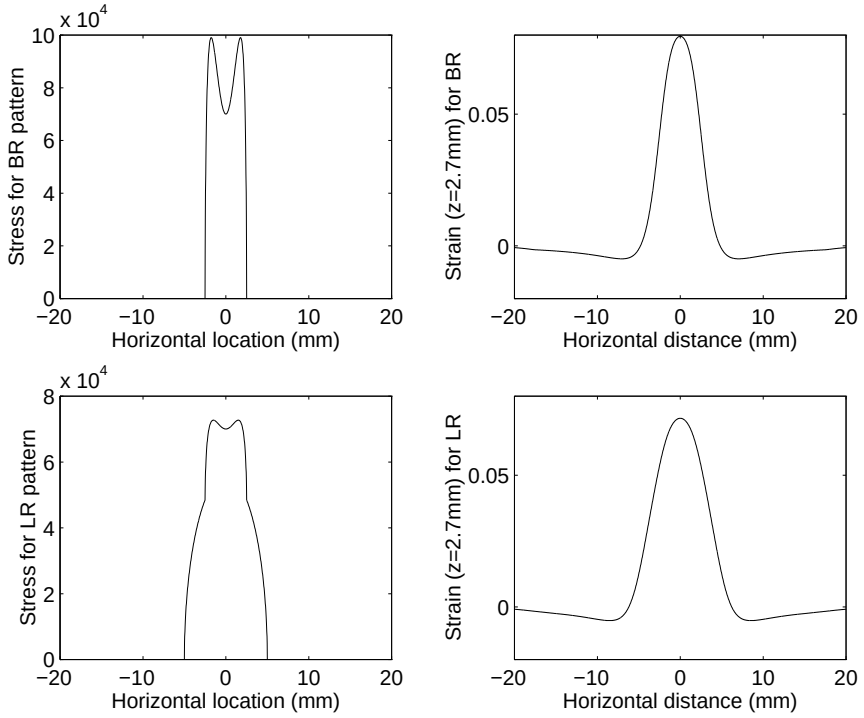

Figure 15: Approximate surface stress and sub-surface strain for big ridge (BR) and little ridge (LR)

where w(x) is the value obtained from the weighting function (figure 14) and $\sigma_{\text{rect}}(x)$ and $\sigma_{\text{cyl}}(x)$ are the stress profiles for the rectangular and cylindrical indentors, respectively. The stress profile for the BR pattern and the corresponding sub-surface strain is shown in the top half of figure 15. Note, the discontinuity present in stress profile for the rectangular indentor has been removed because the edges of the BR pattern were smoothed down. When the BR pattern was pressed against the finger, only the ridge came into contact with the finger. This was very different from the type of contact that resulted when the little-ridge (LR) pattern was indented into the finger. Because the height of the LR was significantly less than the height of the BR, the contact occurred over $10mm$ as opposed to $5mm$ (for the BR). In other words, the finger pulp came into contact with the little-ridge as well as the base of the wax block. The contact with the base of the block was modeled as a cylindrical contact and the contact with the ridge was modeled as a BR contact. Again using superposition, the stress profile for the LR was the weighted (second point above) sum of the stress profile for smooth contact (over $10mm$) and the stress profile of the BR (calculated above). The stress profile and the corresponding sub-surface strain for the LR pattern is shown in the bottom half of figure 15. These

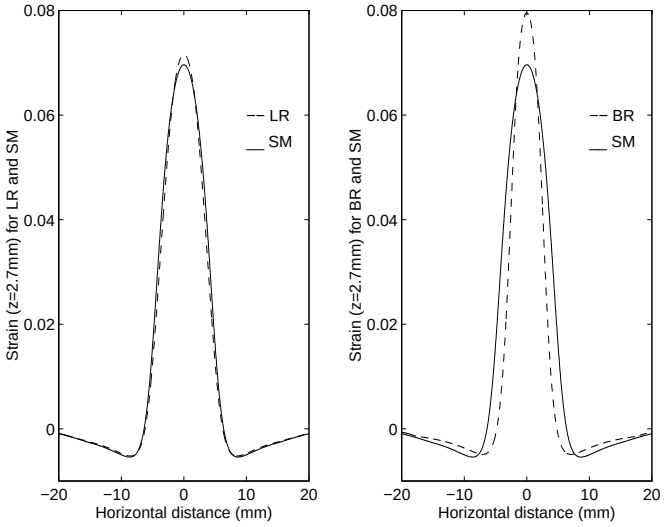

Figure 16: Sub-surface strain for ridged and smooth patterns

contact models are very crude, but the LPF of the $2mm$ glove hides small detail.

Earlier it was mentioned that the height of the LR was picked such that it was at the 50% threshold level for each subject. This contrasted with the BR, which was at the 100% threshold level. Figure 16 gives an explanation based on the skin mechanics (in this case, sub-surface strain), for what caused the difference in the threshold level. The left part of the figure shows the sub-surface strain profile for the LR and SM patterns. It is clear that the sub-surface strain profiles for both these patterns are very similar. Therefore, when the subjects were presented with the LR, they had to guess whether they felt a ridge (and they had a 50% chance of guessing correctly). The right side of figure 16 shows the strain profiles for BR and SM. The BR strain profile is clearly distinguishable from the SM or LR strain profiles. So, when presented with a BR, the subject had no trouble perceiving the ridge.

To explain the effect of hysteresis on tactile perception, we looked at trials of types 4 (LR,BR) and 5 (BR,LR). We will concentrate on trial 5 here because as mentioned above, the BR input had a very distinguishing strain profile and the memory effect of the LR input on it was not very interesting. But, the memory effect of the BR input on the strain profile when the LR input was applied was very important in explaining why the choice2 (two positive ridges felt) means were lower for trials of type 5. In other words, the BR input had a definite influence on the perception of the LR pattern. This influence can be modeled (assuming linearity and thus using superposition)

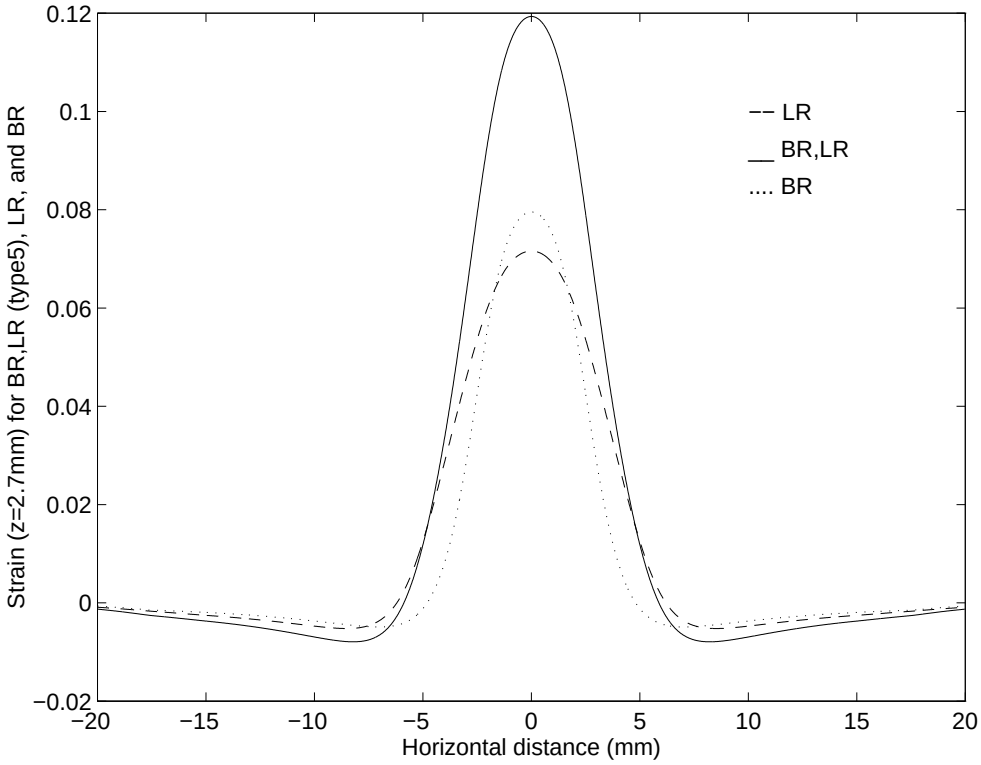

Figure 17: Sub-surface strain for LR, BR and after the second input for type5 (BR,LR) trial at t=1.8 seconds

as follows:

$$\epsilon_{\text{br,lr}} = \epsilon_{\text{lr}} + \alpha(t)\epsilon_{\text{br}} \tag{15}$$

In equation (15), $\alpha(t)$ represents the amount of influence that the BR pattern has on the strain profile of the LR pattern. In our case $t = 1.8$ seconds, since that was the time between the presentation of the BR and the LR patterns. We can think of $\alpha(t)$ as another "measure" of hysteresis or memory in tactile perception. It is unclear as to how one can derive values for $\alpha(t)$. But as a starting point, we chose to average the values of table 4, which contains the percent deformation remaining in the finger 1.8 seconds after a BR pattern is applied. This is a good estimate for $\alpha(1.8)$ if the finger deformation is directly related to the sub-surface strain at the mechanoreceptors (this is probably not the case but it does provide a good starting point). Figure 17 shows the sub-surface strain for trials of type 5 (i.e. LR pattern applied 1.8 seconds after the BR pattern). In the figure, $\alpha(1.8) = 0.6$. The figure also shows the strain at $z = 2.7mm$ for the LR pattern and a BR pattern. Looking at the strain profiles, it is immediately clear that the BR,LR profile is not at all like the LR or the BR profiles. Assuming that the person is using the sub-surface strain information to determine if they

felt two ridges and that the BR,LR profile does not look anything like the profile of a ridge, the hysteresis or memory (measured by $\alpha(t)$) effect explains why the choice2 means were lower for trials of type 5.

Subject 1 does not show any signs of hysteresis. One explanation could be that with $t = 1.8$ seconds, his value for $\alpha(t)$ is very close to zero. Therefore, for trials of type 5, the strain profile for LR (preceded by a BR) is identical to the strain profile of the LR pattern. Subject 1 might show a measurable amount of hysteresis if we used a smaller value for t.

5.2 Sources of Error

There were weaknesses in the experimental apparatus which lead to errors or inconsistencies in the data. The Lord Sensor, with no forces or load on it, had errors up to $0.4N$ while measuring force. In fact, for one subject the standard deviation of the forces applied during the second experiment was $1.5N$. Some subjects were able to use the variance in the force to get extra information. This lead to certain biases in the responses for certain subjects (especially the subjects with prior knowledge of the experimental apparatus and procedures). Another error that could have resulted in biased or incorrect results was the fact that the second experiment was broken up into five sessions. This made the tests more bearable, reducing fatigue. But this resulted in variances in finger position (and where the actual contact was made on the finger) between each sessions.

One other problem with the apparatus was that the finger was not completely immobilized. Since the finger could be moved slightly, this sometimes gave subjects more information to determine if they had felt a ridge or not. Additionally, while running the experiment to measure the viscoelastic parameters of the human finger, any voluntary or involuntary (twitches, etc.) movement of the finger was sensed by the force/torque sensor. This could have resulted in erroneous numbers for the various parameters of the model.

The contact between the wax block containing a pattern and the finger pulp was also subject to slipping. The SAI mechanoreceptors are sensitive mainly to skin surface deformations. But if there is slipping during contact, then the FAI and FAII mechanoreceptors are stimulated. The FAI mechanoreceptors are extremely sensitive to slippage when small features are moved across the surface of the skin. The FAII mechanoreceptors are very sensitive to high frequency vibrations. The rubber layer helped with the vibration damping but again, information other than the surface deformations might have been used to determine the type of pattern presented in each input. Since

this study did not account for those mechanoreceptors, there is no way to gauge what effect they had on the overall tactile perception.

As mentioned in section 2, there were several limitations in the models we used. Fung, and Pawluk have shown that the finger pulp behavior has a better match with a quasi-linear viscoelastic model. Further, at the forces we were working at $5.5N$, it is very possible that there were non-linear effects on the finger that were not modeled. In our model of skin mechanics, we assumed that the rubber and skin form one continuous layer with identical modulus of elasticity. It is known that this is not true. There is actually a discontinuity between the skin and the rubber which our model does not take into account.

5.3 Future Work

In this project, we have shown that tactile perception has a memory effect which could be modeled as arising from viscoelasticity. We assumed that the finger behaved linearly, but a better model might be Fung's quasi-linear viscoelastic model. In the future, we would like to run more tests and determine the parameters of the quasi-linear viscoelastic model. Furthermore, we would like to look at a more holistic model of the finger that included taking into account the action potentials at the mechanoreceptors (i.e., make use of the Hodgkin-Huxley Equations).

The viscoelasticity of the finger does indeed affect the human tactile perception. We have not dealt with the question of the magnitude of this effect. We have also not explored how this effect could be exploited to build better tactile displays. Future experiments could be designed based on similar apparatus and procedures outlined here.

References

[CLF92] M. Cohn, Lam, and R. Fearing. Tactile feedback for teleoperation. *Telemanipulator Technology-SPIE Proceedings 1833*, 1992.

[Con66] H.D. Conway. Normal and shearing contact stresses in indented strips and slabs. *International Journal of Engineering Science*, 4:343–359, 1966.

[Dor89] Clayton L. Van Doren. A model of spatiotemporal tactile sensitivity linking psychophysics to tissue mechanics. *Journal of Acoustical Society of America*, 85(5):2065–2080, 1989.

[Dor90] Clayton L. Van Doren. The effects of a surround on vibrotactile thresholds: Evidence for spatial and temporal independence in the non-Pacinian I (NPI) channel. *Journal of Acoustical Society of America*, 87(6):2655–2661, 1990.

[Fea90] Ronald S. Fearing. Tactile sensing mechanisms. *The International Journal of Robotics Research*, 9(3):3–23, 1990.

[FH85] Ronald S. Fearing and John M. Hollerbach. Basic solid mechanics for tactile sensing. *The International Journal of Robotics Research*, 4(3):40–54, 1985.

[Fun93] Y.C. Fung. *Biomechanics: Mechanical Properties of Living Tissues*. Springer-Verlag, second edition, 1993.

[How97] Robert Howe, April 1997. Personal communication.

[Kon95] Dimitrios Apostolos Kontarinis, May 1995. PhD Thesis.

[Nic94] Edward J. Nicolson. Standardizing I/O for mechatronic systems (sioms) using real time unix device drivers. *Presented at 1994 IEEE International Conference on Robotics and Automation*, 1994.

[PH96a] Dianne Pawluk and Robert Howe. Dynamic contact mechanics of the human fingerpad, part ii: Distributed response. Technical report 96-004, Harvard Robotics Lab, 1996.

[PH96b] Dianne Pawluk and Robert Howe. Dynamic contact mechanics of the human fingerpad, part i: Lumped response. *Submitted to Journal of Biomechanical Engineering*, 1996.

[PH96c] Dianne Pawluk and Robert Howe. A viscoelastic model of the human fingerpad. Technical report 96-003, Harvard Robotics Lab, 1996.

[PJ81] John R. Phillips and Kenneth O. Johnson. Tactile spatial resolution III. a continuum mechanics model of skin predicting mechanoreceptor responses to bars, edges, and gratings. *Journal of Neurophysiology*, 46(6):1204–1225, 1981.

[SJR95] E.R. Serina, C.D. Mote Jr., and D.M. Rempel. Mechanical properties of the fingertip pulp under repeated, dynamic, compressive loading. *ASME Winter Annual Meeting*, 1995.

[Tan95] Eden Tan, August 1995. M.S. Thesis.

[WM93] Ronald Walpole and Raymond Myers. *Probability and Statistics for Engineers and Scientists*. Macmillan Publishing Company, fifth edition, 1993.